Chinese Chemical Letters 36 (2025) 110315

Contents lists available at ScienceDirect

Chinese Chemical Letters

journal homepage: www.elsevier.com/locate/cclet

A 690-nm-excitable type I & II photosensitizer based on biotinylation of verteporfin for photodynamic therapy of deep-seated orthotopic breast tumors

Haoran Hou[a], Siwen Wei[a], Yutong Shao[b], Yingnan Wu[b], Gaobo Hong[a], Jing An[a], Jiarui Tian[b], Jianjun Du[a], Fengling Song[b,*], Xiaojun Peng[a]

[a] State Key Laboratory of Fine Chemicals, Frontiers Science Center for Smart Materials Oriented Chemical Engineering, Dalian University of Technology, Dalian 116024, China
[b] Institute of Frontier Chemistry, School of Chemistry and Chemical Engineering, Shandong University, Qingdao 266237, China

ARTICLE INFO

Article history:
Received 19 April 2024
Revised 26 July 2024
Accepted 31 July 2024
Available online 5 August 2024

Keywords:
Photodynamic therapy
Orthotopic breast tumor
Deep-seated tumor
Type I PDT
Photosensitizers

ABSTRACT

The efficacy of photodynamic therapy (PDT) for breast tumors is hindered by challenges such as inadequate tumor targeting, limited treatment depth, and strong oxygen dependence. Herein, a promising photosensitizer VP-B was developed to simultaneously address all the aforementioned issues for the treatment of hypoxic deep-seated breast tumors. The biotinylated photosensitizer VP-B not only exhibited precise targeting towards breast tumor tissue, but also efficiently triggered the generation of abundant $^1O_2$ and $O_2^{-\bullet}$ under 690 nm red light irradiation. Indeed, the red light penetration ability enabled VP-B to achieve successful application in a mouse orthotopic breast tumor model. After intravenous administration, VP-B can selectively target tumor tissues and significantly inhibit the growth of hypoxic deep-seated tumors. Therefore, this new type I & II photosensitizer could boost fluorescence-guided photodynamic therapy of other hypoxic solid tumors.

Breast cancer is typically characterized by the uncontrolled growth of abnormal cells in the breast tissue. These cells can form a tumor that can invade surrounding tissues and potentially spread to other parts of the body [1-3]. The treatment modalities for breast cancer including surgical intervention, radiation therapy, and chemotherapy often result in various adverse effects among patients due to their invasive ways and systemic toxicity [4-7]. Photodynamic therapy (PDT) is an attractive non-invasive therapeutic approach with less side effects that involves the utilization of specific wavelengths of light to activate photosensitizers [8]. The activated photosensitizers generate reactive oxygen species (ROS) that stimulate cell death mechanisms, inducing tumor cell apoptosis, microvascular damage, and anticancer immune responses [9-11].

Most photosensitizers used in clinical PDT involves type II photochemical reactions process, where the photosensitizers react with oxygen to produce highly toxic singlet oxygen ($^1O_2$) [12,13]. This process, which necessitates the involvement of oxygen, contradicts the hypoxic microenvironment characteristic of tumor cells, thereby exacerbating their heightened oxygen consumption levels and diminishing the efficacy of photodynamic therapy [14]. Besides, many other challenges for tumor PDT photosensitizers remain, including deeper light penetration, more selective absorption or retention in targeting tumors, and more higher biosafety [15].

Verteporfin (VP) is a photosensitizer approved by the Food and Drug Administration (FDA) for the clinical treatment of age-related macular degeneration due to its good biosafety. But it is only used in the field of ophthalmology due to its low selective retention in turmor tissues [16-18], although research is also underway for its use in treating primary breast cancer in clinical trials (NCT02872064) [19,20]. As a promising photosensitizer in PDT, VP exhibits a high triplet quantum yield ($\Phi_T = 0.68$ under N_2 saturation conditions) and a high singlet oxygen quantum yield ($\Phi_\Delta = 0.78$), generating a significant amount of triplet states and singlet oxygen upon 690-nm light excitation [21,22], demonstrating deeper tissue penetration and higher PDT efficiency [23]. These characteristics make VP a promising and safe PDT photosensitizer for deep-seated tumors treatment.

However, the conventional approach of employing VP in PDT still adheres to type II processes, which heavily relies on oxygen and thus restricts treatment efficacy in hypoxic tumor environ-

* Corresponding author.
E-mail addresses: songfl@sdu.edu.cn, songfl@dlut.edu.cn (F. Song).

https://doi.org/10.1016/j.cclet.2024.110315
1001-8417/

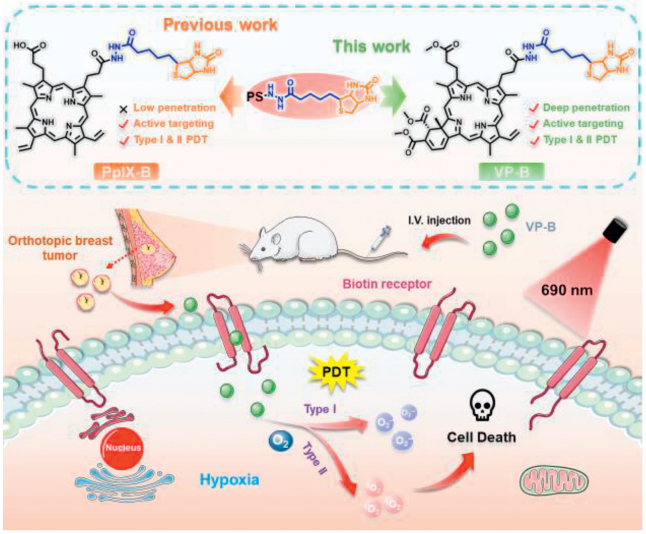

Scheme 1. Schematic illustration of the molecular design of VP-B and photodynamic cancer therapy by type I & II photochemical reactions.

ments [24-26]. Less oxygen-dependant type I PDT photosensitizers are considered to be able to alleviate the limitations of type II PDT photosensitizers [27,28]. In type I photodynamic therapy processes, the excited photosensitizer transfers electrons or hydrogen protons to surrounding substrates, resulting in the generation of free radicals such as $O_2^{-\bullet}$ and $^{\bullet}OH$. Excessive $O_2^{-\bullet}$ is known to react with proteins, DNA, and lipids, causing irreversible damage to cellular components. Importantly, this process involves in $O_2^{-\bullet}$ disproportionation reactions, which can realize the reuse of O_2 [29].

Biotinylation can offer photosensitizers targeting ability for many kinds of tumors, especially for breast tumors [30]. Unexpectedly, a biotinylated porphyrin molecule PpIX-B was reported by our group to simultaneously achieve tumor targeting ability and type I PDT ability [31]. Inspired by PpIX-B, herein, a new photosensitizer VP-B by biotinylation of VP has been designed and developed as a type I & II photosensitizer for targeted deep-seated breast tumors treatment (Scheme 1). Compared with VP, VP-B obtained better tumor targeting and more efficient PDT under hypoxic conditions. Compared to PpIX-B, VP-B exhibited deeper tissue penetration ability benefitting deep-seated breast cancer PDT.

In this study, the photosensitizer VP-B was synthesized by amide condensation of VP with 5-(2-oxo-1,3-dihydro-1*H*-thieno[3,4-*d*]imidazol-4-yl)pentanohydrazide (Fig. S1 in Supporting information). And the chemical structure of VP-B was fully characterized by ^{1}H nuclear magnetic resonance (NMR), ^{13}C NMR, and high resolution mass spectrometry (HRMS) (Figs. S2–S6 in Supporting information). VP-B exhibited absorption and fluorescence spectra (650–750 nm) similar to VP (Fig. S7 in Supporting information). In addition, it displayed a maximum absorption peak at 689 nm, showing a further redshift compared to PpIX-B (Fig. 1a and Fig. S8 in Supporting information), and it could be excited by light with a wavelength of 690 nm (Fig. S9 in Supporting information), indicating its greater potential in deeped-seated tumor treatment. Subsequently, the $^1O_2$ generation of VP-B was evaluated by using 1,3-diphenylisobenzofuran (DPBF, a $^1O_2$ detector) [32]. Under 690-nm red light irradiation, VP-B caused a more significant decrease in absorbance at 415 nm than PpIX-B, indicating better $^1O_2$ production capability than PpIX-B (Fig. S10 in Supporting information). The comparison of $^1O_2$ generation between VP-B and VP showed no significant difference (Fig. 1b and Fig. S11 in Supporting information). The results demonstrated that the coupling of biotin fragment did not impact $^1O_2$ production. The better $^1O_2$

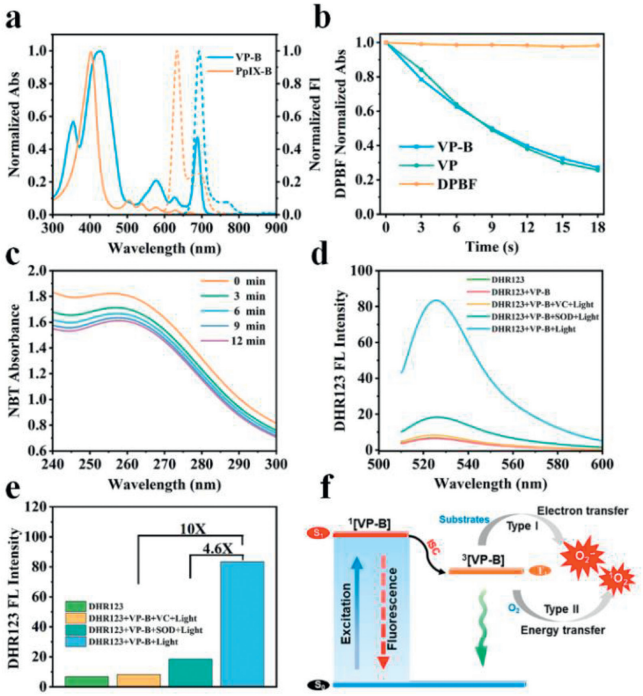

Fig. 1. (a) Normalized UV–vis absorption (solid lines) and fluorescence spectra (dashed lines) of VP-B and PpIX-B in ethanol. (b) Absorbance degradation at 415 nm of DPBF (50 μmol/L) with VP-B(10 μmol/L) and VP (10 μmol/L) as a function of irradiation time (690 nm, 20 mW/cm^2). (c) Photodegradation curves of NBT with VP-B (690 nm, 20 mW/cm^2). (d) Fluorescence spectra of DHR123 as fluorescence probe for $O_2^{-\bullet}$ generation. (e) Fluorescence intensity of DHR123 at 526 nm after 690 nm irradiation for 5 min. (f) Schematic illustration of $^1O_2$ and $O_2^{-\bullet}$ generation mechanism of VP-B.

generation ability of VP-B than PpIX-B was further confirmed using singlet oxygen sensor green (SOSG), a $^1O_2$ fluorescence probe (Fig. S12 in Supporting information) [33]. The above results indicate VP-B keeps the same capacities as VP of 690-nm excitation and $^1O_2$ production as type II photosensitizer.

Next, the capacity of $O_2^{-\bullet}$ generation as type I photosensitizer was evaluated for VP-B by using a specific $O_2^{-\bullet}$ detection probe NBT [34]. As shown in Fig. 1c and Fig. S13 (Supporting information), $O_2^{-\bullet}$ generation was observed in VP-B but not in VP under the same 690-nm light irradiation. This suggests that biotinylation has a positive impact on $O_2^{-\bullet}$ production, which is consistent with our previous study [31]. To further validate the $O_2^{-\bullet}$ generation ability of VP-B, DHR123 was used as a fluorescence probe for $O_2^{-\bullet}$ [35]. As shown in Fig. S14 (Supporting information), we observed the significant increase in fluorescence intensity at 526 nm within 10 min of irradiation, providing compelling evidence for the generation of $O_2^{-\bullet}$. Meanwhile, VP-B exhibited stronger superoxide anion radical generation capability compared to PpIX-B. Moreover, the quenched fluorescence by addition of superoxide dismutase (SOD) or antioxidant vitamin C (Vc) further confirmed the enhanced DHR123 signal was attributed to the generation of $O_2^{-\bullet}$ (Fig. 1d). As expected, the fluorescence intensity showed an 4.9-fold and 10-fold decrease respectively (Fig. 1e). Therefore, we conclude that the photosensitizer VP-B simultaneously engages in two distinct photochemical reactions (Fig. 1f), generating $^1O_2$ through an energy transfer pathway (type II) and producing $O_2^{-\bullet}$ through an electron transfer pathway (type I).

Based on its excellent ability to generate reactive oxygen species in solutions, we subsequently checked the PDT ability of VP-B in breast cancer cells. Initially, we assessed the cellular uptake levels of VP-B by confocal laser scanning microscopy (CLSM) with MCF-7 breast cancer cells and COS-7 normal cells. As shown

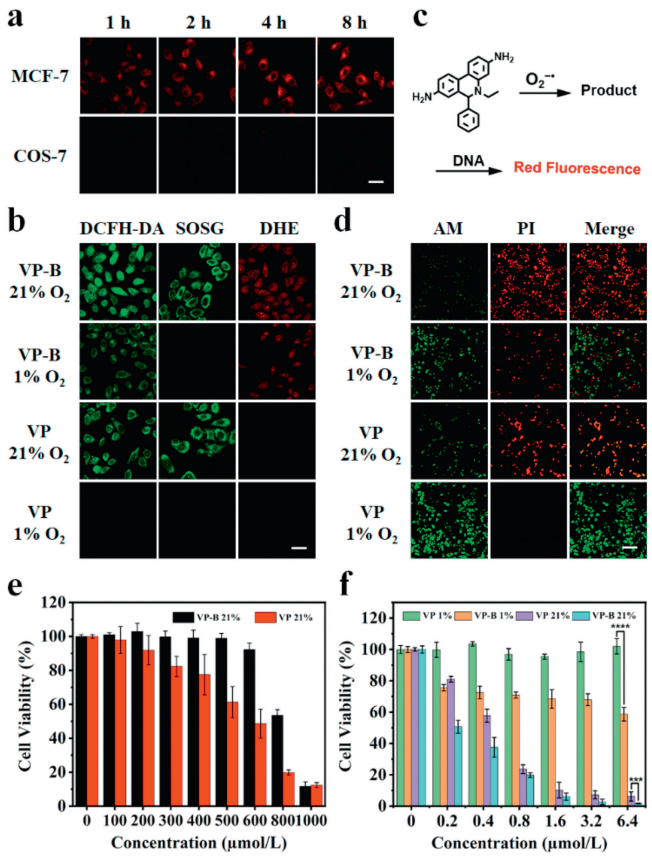

Fig. 2. (a) Cellular uptake imaging of VP-B in MCF-7 and COS-7 cells, respectively. Scale bar: 30 μm. (b) ROS detection in MCF-7 cells under normoxic (21% O_2) or hypoxic (1% O_2) conditions using DCFH-DA, SOSG, and DHE as the ROS, $^1O_2$, and $O_2^{-\bullet}$ fluorescence indicator, respectively (690 nm, 20 mW/cm^2, 3 min). Scale bar: 30 μm. (c) Schematic illustration of DHE for $O_2^{-\bullet}$ detection. (d) Live/dead cell costaining assays using calcein-AM and propidium iodide as fluorescence probes under normoxic (21% O_2) or hypoxic (1% O_2) conditions (690 nm, 20 mW/cm^2, 3 min). Scale bar: 100 μm. (e) Dark toxicity of VP-B and VP on MCF-7 cells under normoxia. Data in (e) are derived from independent biological samples ($n = 5$, mean ± SD). (f) Cell viability of MCF-7 cells treated with increasing concentrations of VP-B and VP after exposure irradiation (690 nm, 20 mW/cm^2, 3 min). Data in (f) are derived from independent biological samples ($n = 5$, mean ± SD, $^{***}P < 0.001$, $^{****}P < 0.0001$).

in Fig. 2a, VP-B can be uptaken by MCF-7 breast cells but not by COS-7 normal cells after 2–4 h. These results support the excellent cellular internalization ability and selectivity of VP-B for breast cancer cells come from the biotin moiety, because the biotin acceptors are over-expreesed by breast turmor cells but not by normal healthy cells. Furthermore, we conducted real-time cellular uptake and subcellular colocalization experiments by incubating VP-B with MCF-7 cells to further investigate the interaction between VP-B and cells. As shown in Figs. S15 and S16 (Supporting information), the red fluorescence intensity gradually increased and reached its maximum after 4 h incubation, which means that the VP-B was uptaken into cells and ultimately enriched in the cytoplasm. Before evaluating the PDT capability of VP-B, we investigated its ROS generation ability *in vitro* living cells. Initially, 2,7-dichlorodihydrofluorescein diacetate (DCFH-DA) was used as ROS fluorescence probe by costaining with photosensitizer in MCF-7 cells under different conditions [36]. As shown in Fig. 2b, under normoxic conditions (21%), both VP and VP-B can produce intracellular ROS levels in MCF-7 cells. However, under hypoxic conditions (1%), ROS generation was only observed in MCF-7 cells which were incubated with VP-B, implying that VP-B may generate alternative types of ROS during hypoxia.

To further investigate the types of ROS generated by VP-B under hypoxic conditions, SOSG and dihydroethidium (DHE) were chosen as $^1O_2$ probe and $O_2^{-\bullet}$ probe, respectively (Fig. 2b). As anticipated, VP-B under hypoxic conditions (1%) cannot generate $^1O_2$ compared with under normoxic conditions (21%) in the SOSG experiments. Consequently, it is plausible that VP-B may generate alternative types of ROS rather than $^1O_2$ under hypoxic conditions. Therefore, the evaluation of $O_2^{-\bullet}$ generation ability was followed by using DHE as $O_2^{-\bullet}$ probe (Fig. 2c) [37]. Remarkably, MCF-7 cells incubated with VP-B exhibited significant red fluorescence under both normoxic conditions (21%) and hypoxic conditions (1%), whereas VP-treated cells did not display notable red fluorescence.

After confirming that VP-B can generate $O_2^{-\bullet}$ in hypoxic cells, the better PDT performance of VP-B than VP for hypoxic cells was visually demonstrated through CLSM experiments by using two fluorescence indicators calcein-AM (green fluorescence for live cells) and propidium iodide (PI, red fluorescence for dead cells). As shown in Fig. 2d, under light exposure, significant red fluorescence of PI was observed in MCF-7 cells treated with VP-B under hypoxic conditions. And green fluorescence of calcein-AM was detected in the VP group under the same hypoxic and irradiation conditions. These results strongly indicate that VP-B holds greater potential than VP in the treatment of hypoxic tumors *via* an oxygen-independent type I PDT pathway.

Subsequently, we employed standard MTT analysis to study the PDT efficacy of VP-B under different conditions. In the absence of light exposure, VP-B exhibited weaker cytotoxicity towards MCF-7 tumor cells than VP (Fig. 2e) under normoxia. The half maximal inhibitory concentration (IC_{50}) value of VP-B was 0.82 mmol/L, and the IC_{50} value of VP was 0.59 mmol/L. The weak dark cytotoxicity of VP-B was also confirmed in COS-7 healthy cells with IC_{50} of 0.73 mmol/L (Fig. S17 in Supporting information). Under red light (690 nm) irradiation at 20 mW/cm^2, the IC_{50} value of VP-B under normoxic conditions (21%) was determined to be 0.25 μmol/L, which is superior to that of VP (IC_{50}= 0.49 μmol/L) (Fig. 2f). The phototoxicity index values (the ratio of IC_{50} of dark cytotoxicity to IC_{50} of phototoxicity) are calculated for VP-B (phototoxicity index = 3263) and VP (phototoxicity index = 1201) to evaluate their potentials as PDT photosensitizers. The higher phototoxicity index value of VP-B indicates that VP-B is the better one than VP. Importantly, VP-B demonstrated potent cytotoxic effects under hypoxic conditions, whereas VP failed to exhibit any killing effect under the same hypoxic conditions. Meanwhile, under normoxic conditions (21%), PpIX-B exhibited poorer phototoxicity (IC_{50} = 2.23 μmol/L) under red light (630 nm) irradiation at 20 mW/cm^2, while under hypoxic conditions, VP-B also showed better phototoxicity than PpIX-B (Fig. S18 in Supporting information). The findings suggested that VP-B has a competitive advantage in PDT compared to PpIX-B. Besides, confocal fluorescence imaging experiments were used to further visually reveal the photocytotoxicity of VP-B with MCF-7 cells by dual-staining with annexin V-fluorescein isothiocyanate (FITC) and PI, regardless of whether in normoxic conditions (21%) or hypoxic conditions (1%) (Fig. S19 in Supporting information). The PDT effect of VP-B were also investigated by the flow cytometry analysis (Fig. S20 in Supporting information). These results suggested that VP-B could induce cellular apoptosis under both normoxic conditions (21%) and hypoxic conditions (1%) [38].

PDT has been demonstrated to induce immunogenic cell death in tumour cells [39], thereby enhancing their immunogenicity and promoting the release of damage-associated molecular patterns (DAMPs) such as calreticulin (CRT) and high mobility group box-1 protein (HMGB1) [40]. Consequently, PDT with VP-B induced immunogenic cell death were vertified with MCF-7 cells upon 690 nm light irradiation. As shown in Fig. S21 (Supporting information), the immunofluorescence imaging data revealed that weak CRT sig-

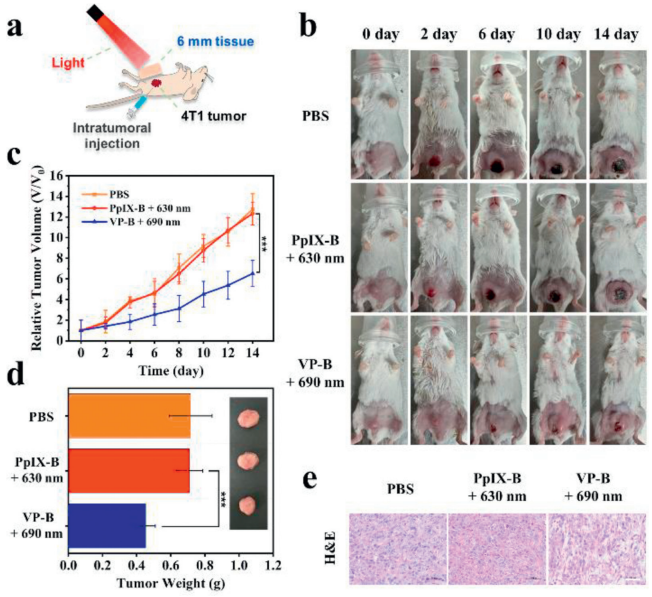

Fig. 3. Photodynamic antitumor efficacy on deep-seated orthotopic breast tumors. (a) Schematic illustration of PDT in simulated hypoxic deep-seated tumors with a cover of 6-mm thickness chicken meat slice. (b) Comparison chart of the treatment effectiveness of orthotopic deep-seated breast tumors for 14 days. (c) Relative tumor volumes of mice after different treatments ($n = 3$, mean ± SD, $^{***}P < 0.001$). (d) Average weight of tumors for mice at 14 days post-treatment ($n = 3$, mean ± SD, $^{***}P < 0.001$). (e) H&E stained images of tumor tissues in mice dissected after 14 days of treatments in different groups. Scale bar: 50 μm.

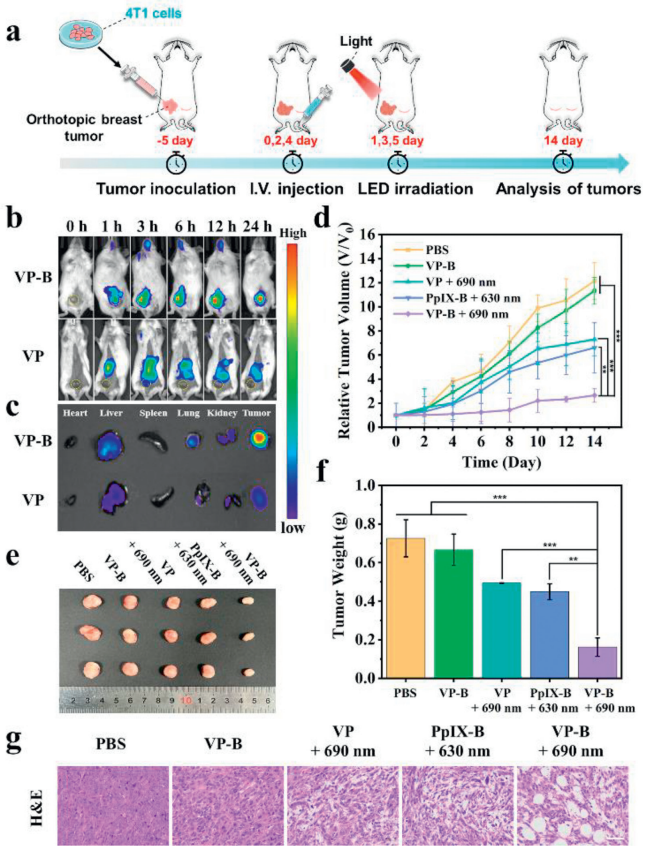

Fig. 4. *In vivo* real time fluorescence imaging and antitumor efficacy in mice with *in situ* breast tumor after iv injection. (a) Treatment timeline for mice with orthotopic breast tumor breast tumor inoculation to the end of treatment. (b) Real time fluorescence imaging of mice with *in situ* breast tumor after intravenous injection of VP-B or VP. (c) Fluorescence imaging of the major organs of mice sacrificed at 24 h post-injection of VP-B or VP. (d) Relative tumor volumes of mice after different treatments ($n = 3$, mean ± SD, $^{**}P < 0.01$, $^{***}P < 0.001$). (e) Tumor tissue of mice dissected after 14 days of treatments in different groups. (f) Average weight of tumors in mice dissected after 14 days of treatments in different groups ($n = 3$, mean ± SD, $^{**}P < 0.01$, $^{***}P < 0.001$). (g) H&E stained images of tumor tissues in mice dissected after 14 days of treatments in different groups. Scale bar: 50 μm.

nals and strong HMGB1 signals in MCF-7 were observed when incubated with VP-B in the absence of light. However, significantly increased CRT signals were observed on the cell surface after light irradiation regardless of normoxic conditions (21%) or hypoxic conditions (1%), indicating enhanced translocation and exposure of CRT on the cell membrane. Meanwhile, the decrease of HMGB1 signal indicated that the migration of HMGB1 from the nucleus to the cytoplasm upon irradiation. These findings suggested that VP-B could induce immunogenic cell death (ICD) in MCF-7 cells upon light irradiation.

Considering the pronounced PDT effect of VP-B *in vitro*, we further explored its *in vivo* anti-tumor potential with mice experiments. All animal experiments were performed based on the protocols approved by the Ethical Committee of Shandong University under production license number SCXK 2019–0001 and use license number SYXK 2019–0005. Initially, the deeper light penetration of VP-B than PpIX-B were confirmed with BALB/c female mice bearing orthotopic breast tumors. A chicken meat slice (6-mm thickness) was placed over the tumor to simulate deep-seated tumors [41], followed by light exposure (30 mW/cm^2, 10 min) (Fig. 3a). The mice with orthotopic breast tumors were randomly divided into three groups (Fig. 3b) which were injected intratumorally with phosphate-buffered saline (PBS, control), PpIX-B (630 nm irradiation), and VP-B (690 nm irradiation), respectively. From the PDT data shown in Fig. 3c, the PpIX-B group with 630-nm irradiation did not delay any tumor growth when compared with PBS group. Expectedly, the VP-B group with 690-nm irradiation exhibited significant tumor suppression, which highlights the PDT effect of VP-B on deep-seated tumors. The average tumor weight and corresponding tumor photographs further substantiated the anti-tumor outcomes of VP-B (Fig. 3d). After euthanasia was performed for those mice, tumor tissues from each group were stained with hematoxylin and eosin (H&E). Histological analysis revealed a significant presence of apoptosis and necrosis for the VP-B group with 690-nm irradiation within the tumor tissue sections (Fig. 3e), indicating the remarkable potential of VP-B for the treatment of deep-seated breast tumors.

To further investigate the advantages of VP-B in overcoming PDT limitations in breast tumors, its PDT effects on 4T1 orthotopic breast tumors of BALB/c mice were studied *via* intravenous injection of the photosensitizers (Fig. 4a). Specific tumor-targeting ability is crucial for accurate PDT. We initially conducted fluorescence imaging through intravenous injections to study the time-dependent distribution of VP-B and VP in mice (Fig. 4b). The results demonstrated that the tumor sites were clearly identifiable from 3 h to 24 h after adminstration with VP-B (Fig. S22 in Supporting information). In contrast, much weaker fluorescence signals were detected with the VP group at the breast tumor locations throughout the observation period. Subsequent dissection of the main organs and tumors from mice for *ex vivo* fluorescence imaging further confirmed the much better targeting and retention capability of VP-B than that of VP (Fig. 4c and Fig. S23 in Supporting information). These results indicate that VP-B can selectively accumulate in breast tumors, benefiting from the outstanding tumor-targeting ability of biotin.

Then, the *in vivo* PDT of orthotopic breast tumors of BALB/c mice was investigated by measuring tumor size after three tail-vein injections of photosensitizers and three times of irradiation (Fig. 4d). After treatment, only the VP-B group with irradiation ex-

hibited a near-complete regression, indicating the best tumor suppression effect. The data of tumor size (Fig. 4e) and average tumor weight (Fig. 4f) from dissected mice also confirmed the outstanding tumor suppression capability of VP-B. The results of H&E staining further confirmed the excellent therapeutic effect of VP-B (Fig. 4g). Compared to the other groups, the VP-B light group exhibited significant tumor tissue necrosis and apoptosis. In the end, the biosafety of these photosensitizers were evaluated by mice body weight (Fig. S24 in Supporting information) and H&E staining analysis of major organs through (Fig. S25 in Supporting information). The results of hemolysis experiments (Fig. S26 in Supporting information) suggested that VP-B with different concentrations (0–100 μmol/L) did not show apparent hemolysis [42]. These results indicated that VP-B has high biosafety.

In conclusion, we have developed a novel type I & II photosensitizer VP-B based on bintinylation of VP to enhance the PDT performance against hypoxic deep-seated tumors. VP-B was demonstrated with successful PDT for orthotopic breast tumors in mice. In a word, VP-B gained a multifaceted therapeutic effect equivalent to "killing three birds with one stone": excellent tumor-targeting ability, deeper light penetration ability and potent $O_2^{-\bullet}$ generation capability. All the three capabilitier of VP-B are crucial for its efficient PDT of deep-seated orthotopic breast tumors. Besides, VP-B was found to have better biosafety than VP. We believe that this study presents a groundbreaking PDT paradigm for all kind of deep-seated solid tumors, and offers invaluable insights for future advancements in cancer therapy and clinical applications.

Declaration of competing interest

The authors declare that they have no known competing financial interests or personal relationships that could have appeared to influence the work reported in this paper.

CRediT authorship contribution statement

Haoran Hou: Writing – original draft, Methodology, Formal analysis, Data curation, Conceptualization. **Siwen Wei:** Visualization, Validation, Methodology, Data curation. **Yutong Shao:** Software, Methodology, Formal analysis. **Yingnan Wu:** Software, Formal analysis. **Gaobo Hong:** Validation, Software, Investigation, Formal analysis. **Jing An:** Visualization, Formal analysis, Conceptualization. **Jiarui Tian:** Methodology, Formal analysis, Data curation. **Jianjun Du:** Resources, Project administration, Funding acquisition. **Fengling Song:** Writing – review & editing, Supervision, Resources, Project administration, Methodology, Investigation, Funding acquisition, Formal analysis, Conceptualization. **Xiaojun Peng:** Supervision, Software, Resources, Project administration, Funding acquisition.

Acknowledgments

This work was supported financially by the National Key Research and Development Program of China (No. 2023YFC3403000), the National Natural Science Foundation of China (No. 22378231), and the Guangdong Basic and Applied Basic Research Foundation (No. 2024A1515012493). We thank Jingyao Qu, Jing Zhu and Zhifeng Li of the Core Facilities for Life and Environmental Sciences, State Key laboratory of Microbial Technology of Shandong University for LC-MS and CLSM analysis.

Supplementary materials

Supplementary material associated with this article can be found, in the online version, at doi:10.1016/j.cclet.2024.110315.

References

[1] A.D. Papanastasiou, C. Sirinian, E. Plakoula, et al., J. Clin. Oncol. 34 (2016) e13011.
[2] P. Pathak, A.S. Jalal, R. Rai, Curr. Med. Imaging 17 (2021) 720–740.
[3] Y. Zhang, Y. Zhang, W. Gao, et al., Int. J. Biol. Macromol. 164 (2020) 3171–3178.
[4] N. Harbeck, M. Gnant, Lancet 389 (2017) 1134–1150.
[5] N. Harbeck, F. Penault-Llorca, J. Cortes, et al., Nat. Rev. Dis. Primers 5 (2019) 66.
[6] S. Loibl, P. Poortmans, M. Morrow, C. Denkert, G. Curigliano, Lancet 397 (2021) 1750–1769.
[7] A.G. Waks, E.P. Winer, JAMA 321 (2019) 316.
[8] P. Agostinis, K. Berg, K.A. Cengel, et al., CA Cancer J. Clin. 61 (2011) 250–281.
[9] J. Oliveira, E. Monteiro, J. Santos, et al., J. Clin. Oncol. 35 (2017) e14056.
[10] D.E.J.G.J. Dolmans, D. Fukumura, R.K. Jain, Nat. Rev. Cancer 3 (2003) 380–387.
[11] A.P. Castano, P. Mroz, M.R. Hamblin, Nat. Rev. Cancer 6 (2006) 535–545.
[12] T.C. Pham, V.N. Nguyen, Y. Choi, S. Lee, J. Yoon, Chem. Rev. 121 (2021) 13454–13619.
[13] X. Zhao, J. Liu, J. Fan, H. Chao, X. Peng, Chem. Soc. Rev. 50 (2021) 4185–4219.
[14] Y.Y. Zhao, H. Kim, V.N. Nguyen, et al., Coord. Chem. Rev. 501 (2024) 215560.
[15] W. Fan, P. Huang, X. Chen, Chem. Soc. Rev. 45 (2016) 6488–6519.
[16] S.G. Bown, BMJ 316 (1998) 754–757.
[17] T.J. Dougherty, C.J. Gomer, B.W. Henderson, et al., J. Natl. Cancer Inst. 90 (1998) 889–905.
[18] U. Schmidt-Erfurth, T. Hasan, Surv. Ophthalmol. 45 (2000) 195–214.
[19] D.S. Pellosi, A.L. Tessaro, F. Moret, et al., J. Photochem. Photobiol. A: Chem. 314 (2016) 143–154.
[20] D.S. Pellosi, L.B. Paula, M.T. de Melo, A.C. Tedesco, Mol. Pharm. 16 (2019) 1009–1024.
[21] K.J. Mellish, S.B. Brown, Expert Opin. Pharmacother. 2 (2001) 351–361.
[22] B. Aveline, T. Hasan, R.W. Redmond, Photochem. Photobiol. 59 (1994) 328–335.
[23] A. Greco, G. Garoffolo, E. Chiesa, et al., J. Drug Deliv. Sci. Technol. 64 (2021) 102562.
[24] A. Sulaiman, S. McGarry, S. El-Sahli, et al., Mol. Cancer Ther. 18 (2019) 1755–1764.
[25] I. Rizvi, S. Nath, G. Obaid, et al., Photochem. Photobiol. 95 (2019) 419–429.
[26] L. Yu, Z. Liu, W. Xu, et al., Acta Pharm. Sin. B 14 (2024) 1111–1131.
[27] J. Tian, B. Li, F. Zhang, et al., Angew. Chem. Int. Ed. 62 (2023) e202307288.
[28] M. Zhao, Y. Zhang, J. Miao, et al., Adv. Mater. 36 (2024) 2305243.
[29] D. Chen, Q. Xu, W. Wang, et al., Small 17 (2021) 2006742.
[30] S. Maiti, P. Paira, Eur. J. Med. Chem. 145 (2018) 206–223.
[31] J. An, S. Tang, G. Hong, et al., Nat. Commun. 13 (2022) 2225.
[32] Y. Shao, M. Chen, W. Chen, et al., Adv. Healthc. Mater. 12 (2023) 2300503.
[33] L.L. Wu, X. Meng, Q. Zhang, et al., Chin. Chem. Lett. 35 (2024) 108663.
[34] S. Obregón, M.A. Ruíz-Gómez, D.B. Hernández-Uresti, J. Colloid Interface Sci. 506 (2017) 111–119.
[35] Y. Zhang, Y. Jiao, X. Jia, Q. Guo, C. Duan, Chin. Chem. Lett. 35 (2024) 108748.
[36] S. Chen, Y. Liu, R. Liang, et al., Chin. Chem. Lett. 32 (2021) 3903–3906.
[37] M. Li, J. Xia, R. Tian, et al., J. Am. Chem. Soc. 140 (2018) 14851–14859.
[38] X. Xing, E. Pang, S. Zhao, et al., Chin. Chem. Lett. 35 (2024) 108467.
[39] Z. Li, X. Lai, S. Fu, et al., Sci. Adv. 9 (2022) 2201734.
[40] C. Yang, M. Wang, M. Chang, et al., J. Am. Chem. Soc. 145 (2023) 7205–7217.
[41] M. Li, T. Xiong, J. Du, et al., J. Am. Chem. Soc. 141 (2019) 2695–2702.
[42] W. Su, X. Luo, P. Li, et al., Chin. Chem. Lett. 35 (2024) 109522.